

REDISCUSSION OF ECLIPSING BINARIES. PAPER XIV.
THE F-TYPE SYSTEM V570 PERSEI

By John Southworth

Astrophysics Group, Keele University, Staffordshire, ST5 5BG, UK

V570 Per is a binary star system containing two F-type stars in a 1.90 d period circular orbit. It shows shallow partial eclipses that were discovered from its *Hipparcos* light curve. We present an analysis of this system based on two sectors of high-quality photometry from the NASA Transiting Exoplanet Survey Satellite (TESS) mission, and published spectroscopic light ratio and radial velocity measurements. We find masses of 1.449 ± 0.006 and $1.350 \pm 0.006 M_{\odot}$, and radii of 1.538 ± 0.035 and $1.349 \pm 0.032 R_{\odot}$. The radius measurements are set by the spectroscopic light ratio and could be improved by obtaining a more precise light ratio. The eclipses in the TESS data arrived 660 ± 30 s later than expected, suggesting the presence of a faint third body on a wider orbit around the eclipsing system. Small trends in the residuals of the fit to the TESS lightcurve are attributed to weak starspots. The distance to the system is close to the *Gaia* DR3 value, but the *Gaia* spectroscopic orbit is in moderate disagreement with the results from the published ground-based data.

Introduction

Detached eclipsing binary stars (dEBs) are our main source of measurements of the physical properties of normal stars. The number of dEBs for which precise measurements are available is increasing gradually, as traced by reviews of this subject¹⁻³ as well as compiled catalogues⁴⁻⁶. The Detached Eclipsing Binary Catalogue (DEBCat*, ref.⁶) currently lists just over 300 dEBs for which masses and radii are measured to 2% precision or better, helped by the widespread availability of light curves from space telescopes⁷.

dEBs are useful in understanding the physical processes that govern the structure and evolution of stars. They have been used to calibrate the amount of convective core overshooting⁸⁻¹⁰ albeit with conflicting results¹¹, the size of the convective core in massive stars¹², mixing length¹³, and the radii of low-mass stars^{14,15}. They are also sources of distance measurements which have been used to calibrate the cosmological distance scale^{16,17}

We are currently pursuing a project to increase the number of dEBs with reliable measurements of their masses and radii¹⁸, primarily using new observations from the NASA Transiting Exoplanet Survey Satellite (TESS) mission¹⁹. TESS has observed thousands of dEBs²⁰⁻²², many of which have available high-quality

*<https://www.astro.keele.ac.uk/jkt/debcats/>

Table I: *Basic information on V570 Per.*

| <i>Property</i> | <i>Value</i> | <i>Reference</i> |
|--------------------------------|-------------------------|------------------|
| Right ascension (J2000) | 03:09:34.94 | 27 |
| Declination (J2000) | +48:38:28.7 | 27 |
| Henry Draper designation | HD 19457 | 28 |
| <i>Hipparcos</i> designation | HIP 1673 | 29 |
| <i>Gaia</i> DR3 designation | 435997252803241856 | 27 |
| <i>Gaia</i> DR3 parallax | 8.2952 ± 0.0355 mas | 27 |
| TESS Input Catalog designation | TIC 116991977 | 30 |
| <i>B</i> magnitude | 8.55 ± 0.02 | 31 |
| <i>V</i> magnitude | 8.09 ± 0.01 | 31 |
| <i>J</i> magnitude | 7.160 ± 0.026 | 32 |
| <i>H</i> magnitude | 6.948 ± 0.017 | 32 |
| <i>K_s</i> magnitude | 6.882 ± 0.020 | 32 |
| Spectral type | F3 V + F5 V | 26 |

radial velocity (RV) measurements. In this context, we present an analysis of the V570 Persei system.

V570 Per (Table I) is an F-type dEB which was discovered using data from the *Hipparcos* satellite²³ and given its variable-star name by Kazarovets et al.²⁴. It was selected for analysis by Munari et al.²⁵ in the context of assessing the expected performance of the *Gaia* satellite in the study of dEBs. These authors used the *Hipparcos* photometry of V570 Per along with ground-based spectroscopy restricted to the 850–875 nm wavelength range to mimic the expected characteristics of the *Gaia* observations. They measured the masses of the components of V570 Per to 2.5%, and the radii to low precisions of 10% and 25% due to the large scatter in the *Hipparcos* data and the shallow eclipses shown by this dEB. Tomasella et al.²⁶ (hereafter T08) presented a more detailed study of V570 Per based on new ground-based photometry, and the same spectroscopy but this time using the full available 450–948 nm wavelength range. They constrained the model of the light curve using spectroscopically-measured light contributions of the two stars in the *V*-band. They determined the atmospheric parameters of the component stars via a χ^2 fit of synthetic spectra to their observed spectra, a process which neglected the systematic errors inherent in this method.

Observational material

The TESS mission¹⁹ observed V570 Per in sectors 18 (2019/11/02 to 2019/11/27) and 58 (2022/10/29 to 2022/11/26), in both cases in short cadence mode with a 120 s sampling rate. We used the LIGHTKURVE package³³ to download these data and reject points flagged as bad. The simple aperture photometry (SAP) and pre-search data conditioning SAP (PDCSAP) data³⁴ are almost indistinguishable, so we used the SAP data in our analysis for consistency with previous papers in this series.

We converted the data to differential magnitude and subtracted the median

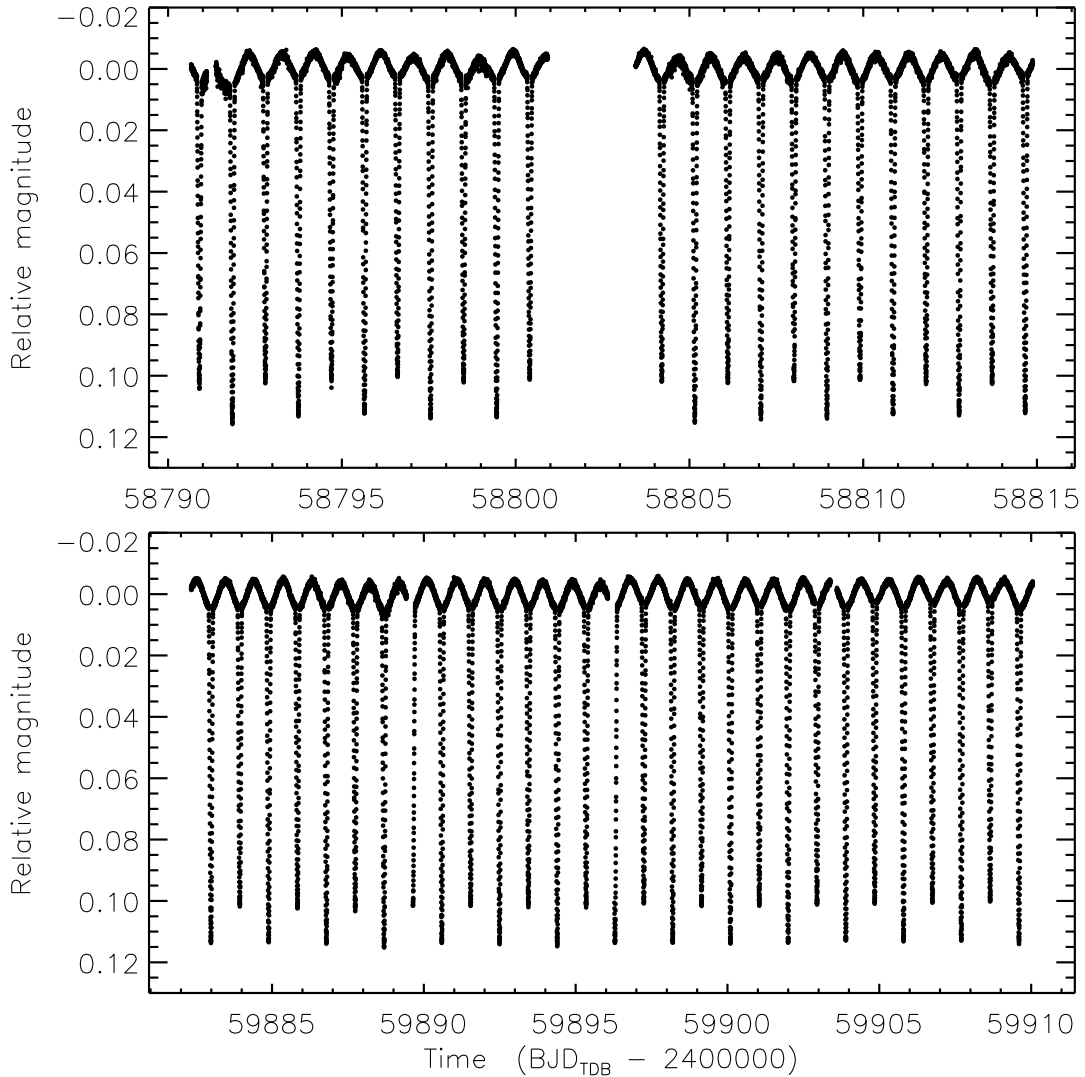


FIG. 1: TESS short-cadence SAP photometry of V570 Per from sectors 18 (top), and 58 (bottom). The flux measurements have been converted to magnitude units then rectified to zero magnitude by subtraction of the median.

magnitude for further analysis, ending up with 15 256 datapoints from sector 18 and 19 475 from sector 58. On further inspection we found that the first stretches of data from both halves of the sector 18 light curve were affected by instrumental systematics, so we trimmed them by removing data in the intervals $[2458790.6, 2458792.5]$ and $[2458801.0, 2458804.7]$. This left a total of 32 719 datapoints over both TESS sectors (Fig. 1).

We queried the *Gaia* DR3 database[†] for objects within 2 arcmin of V570 Per. A total of 108 were found, all of which are fainter than V570 Per by at least 7.2 mag in the *Gaia* *G* band. We deduce that the amount of light contaminating the TESS aperture for this dEB is negligible.

[†]<https://vizier.cds.unistra.fr/viz-bin/VizieR-3?-source=I/355/gaiadr3>

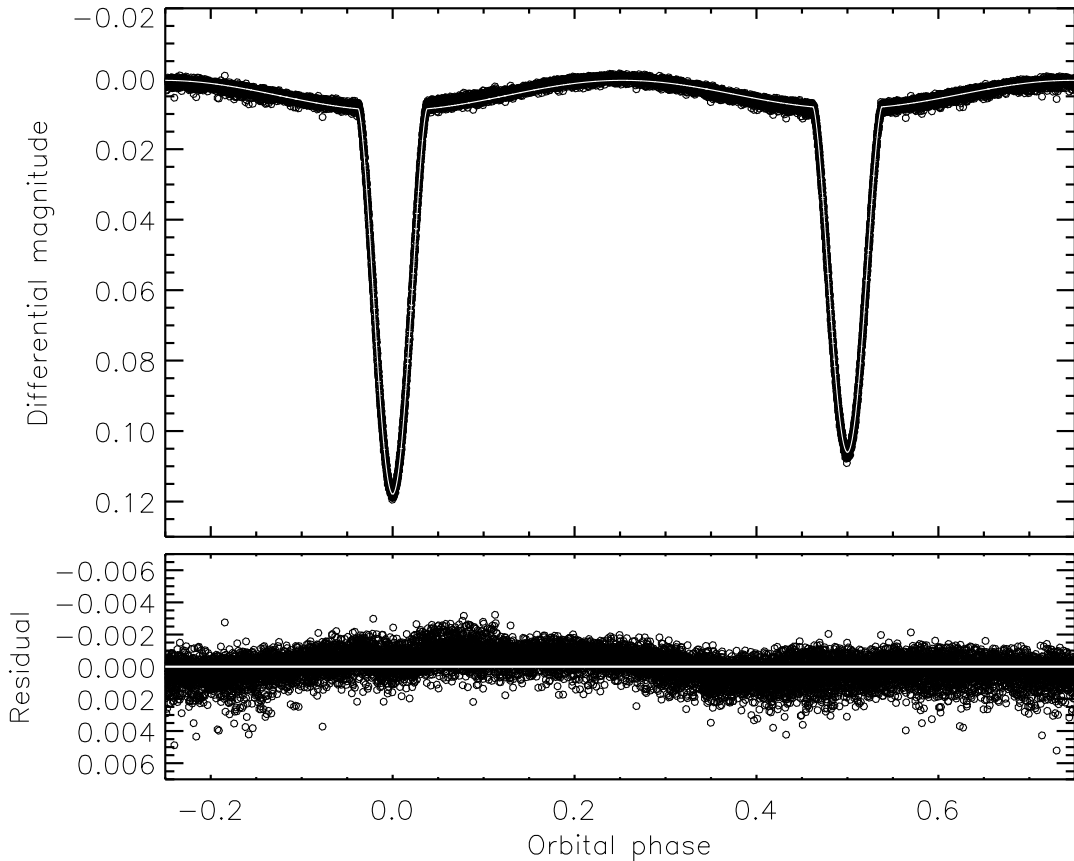


FIG. 2: Best fit to the TESS sector 18 light curve of V570 Per using JKTEBOP as a function of orbital phase. The residuals are shown on an enlarged scale in the lower panel.

Light curve analysis

We modelled the light curves from the two sectors both individually and together, using version 43 of the JKTEBOP[‡] code^{35,36}. In all cases the parameters of the fit included the fractional radii of the stars (r_A and r_B), expressed as their sum ($r_A + r_B$) and ratio ($k = r_B/r_A$), the orbital inclination (i), the central surface brightness ratio (J), the ephemeris (period P and reference time of primary minimum T_0) and the coefficients of the reflection effect. We define star A to be the one eclipsed at the deeper minimum and star B to be its companion. A circular orbit was assumed based on the appearance of the light curve and of the RVs presented by T08 – when allowing for an eccentric orbit we found a best-fitting eccentricity of $e = 0.0053$ and almost no change in the other parameters. We included a quadratic function versus time for each half-sector to account for slow changes in the brightness of the dEB due to instrumental effects.

The eclipses are partial and shallow, so the light curve solution suffers from a strong degeneracy between k , i and J (e.g. refs.³⁷ and³⁸). This effect was found by T08 when modelling their ground-based photometry, and remains present in the much more extensive and higher-precision TESS data used in the current

[‡]<http://www.astro.keele.ac.uk/jkt/codes/jktebop.html>

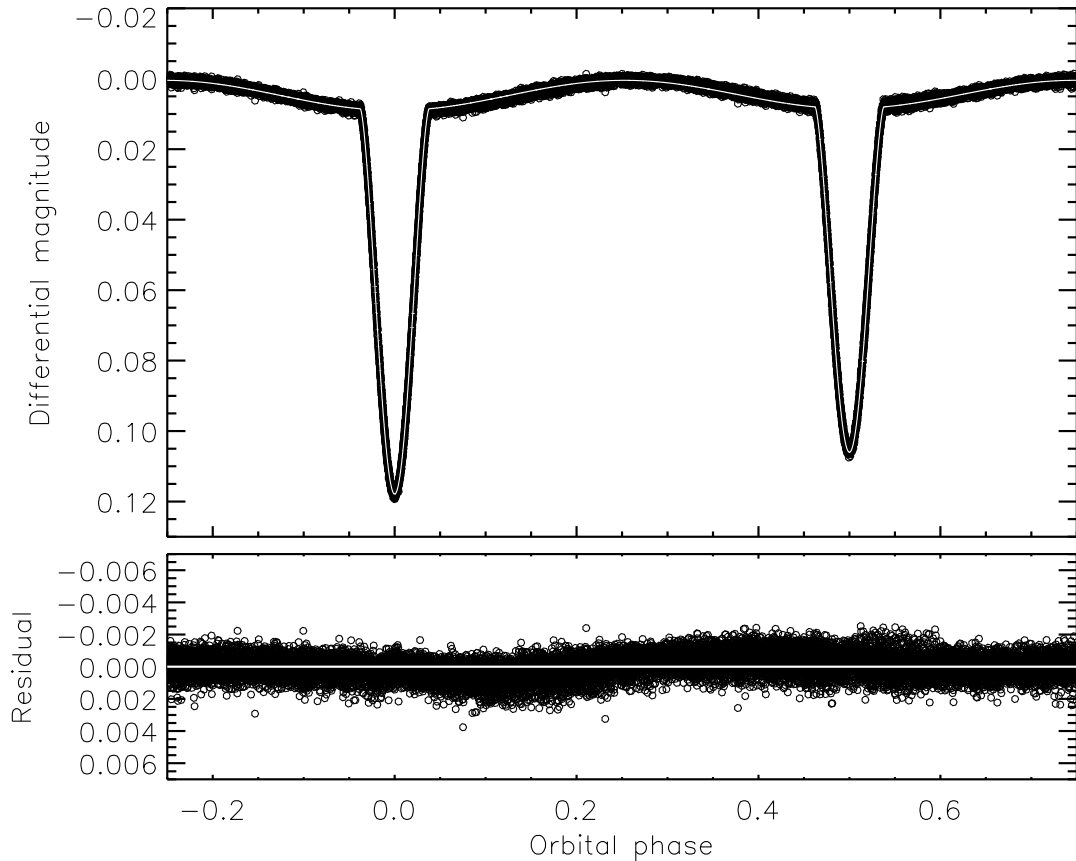


FIG. 3: Best fit to the TESS sector 58 light curve of V570 Per using JKTEBOP as a function of orbital phase. The residuals are shown on an enlarged scale in the lower panel.

study. We therefore applied a spectroscopic light ratio as a constraint, in the same way as done in our work on V1022 Cas³⁹ and HD 23642⁴⁰. The light contributions found by T08 correspond to a light ratio of $\ell_B/\ell_A = 0.667 \pm 0.053$ in the V -band. We propagated this to the TESS passband using the response function from Ricker et al.¹⁹, theoretical spectra from Allard et al.⁴¹, and the effective temperature (T_{eff}) values from T08, finding $\ell_B/\ell_A = 0.703 \pm 0.057$.

Limb darkening (LD) was included in the fit⁴² using the power-2 law⁴³ and theoretical LD coefficients⁴⁴. Fitting for the scaling coefficient (“ c ” in the terminology of Maxted⁴⁵) for both stars yielded determinate values and little change in the other parameters, so was adopted as the default approach.

The amount of third light (L_3) has a significant effect on the best-fitting parameter values. If fitted, it converges to a formally significant but unphysically negative value (-0.083 ± 0.018) despite the negligible amount of light from nearby stars (see previous section). We therefore fixed it at zero in our default solution, but added contributions to the errorbars based on the change in parameter values by assuming $L_3 = 2\%$ instead. For information, such an assumption decreases r_A by 1.1% and increases r_B by 0.4%.

The best fits to the light curves from the two sectors are shown in Figs. 2 and 3. These plots show the result of a fit to both sectors simultaneously, but divided

Table II: Adopted parameters of V570 Per measured from the TESS light curves using the JKTEBOP code. The uncertainties are 1σ and were determined using Monte Carlo and residual-permutation simulations.

| <i>Parameter</i> | <i>Value</i> |
|---|-------------------------------|
| <i>Fitted parameters:</i> | |
| Time of primary eclipse (BJD _{TDB}) | $2459894.392999 \pm 0.000009$ |
| Orbital period (d) | $1.90093830 \pm 0.00000002$ |
| Orbital inclination ($^\circ$) | 77.294 ± 0.048 |
| Sum of the fractional radii | 0.31715 ± 0.00057 |
| Ratio of the radii | 0.877 ± 0.036 |
| Central surface brightness ratio | 0.8767 ± 0.0033 |
| LD coefficient c for star A | 0.548 ± 0.017 |
| LD coefficient c for star B | 0.516 ± 0.020 |
| LD coefficient α for star A | 0.498 (fixed) |
| LD coefficient α for star B | 0.467 (fixed) |
| Orbital eccentricity | 0.0 (fixed) |
| <i>Derived parameters:</i> | |
| Fractional radius of star A | 0.1690 ± 0.0028 |
| Fractional radius of star B | 0.1482 ± 0.0035 |
| Light ratio ℓ_B/ℓ_A | 0.683 ± 0.060 |

into individual sectors in the plots. Slow trends in the residuals are apparent in both cases, and are discussed below.

The fitted parameters are given in Table II. Uncertainties in the parameters were determined using Monte Carlo and residual-permutation simulations^{46,47}. The Monte Carlo errorbars are significantly larger than the residual-permutation alternatives because the latter do not account for the uncertainty in the spectroscopic light ratio. We therefore adopted the Monte Carlo errorbars for all parameters. The dominant source of uncertainty is the spectroscopic light ratio, which could be improved by further observations and analysis.

The out-of-eclipse variability

The best fits to the light curves (Figs. 2 and 3) show slow trends in the residuals which differ between the two sectors. Our preferred interpretation of this is small brightness variations present on the surface of one or both stars, with the star(s) rotating synchronously with the orbit in order to obtain the consistent phasing in Figs. 2 and 3. This could be caused by starspots, and evolution of the spot configuration is a natural explanation for the differences between the residuals of the fits to the two sectors. The T_{eff} values of the stars are relatively high for this explanation, but are only slightly higher than KIC 5359678 for which spot activity was clearly detected^{48,49}. The lack of increased residuals during eclipse suggests the spots are either a similar temperature to the rest of the photosphere and/or are located on parts of the star(s) that are not eclipsed.

We checked for the possibility of pulsations by calculating a periodogram of the residuals of the fit to the data from sector 58, using the PERIOD04 code⁵⁰.

Significant signals were found at the orbital period and half the orbital period, in agreement with the starspot hypothesis. No evidence for either δ Scuti or γ Doradus pulsations were found, despite a significant number of such pulsators now being known in dEBs^{51–55}.

Radial velocities

T08 measured RVs of both stars from each of 31 high-quality échelle spectra obtained using the Asiago 1.8 m telescope. We obtained these from table 2 in T08 and modelled them using JKTEBOP, adopting a circular orbit and separate systemic velocities (V_γ) for the two stars. We fitted for velocity amplitudes (K_A and K_B), $V_{\gamma,A}$, $V_{\gamma,B}$ and T_0 . The period was fixed at the value from Table II. Uncertainties were calculated from 1000 Monte Carlo simulations^{35,56} after adjusting the sizes of the errorbars to give a reduced χ^2 of unity for the RVs for each star.

We found $K_A = 113.94 \pm 0.24 \text{ km s}^{-1}$, $K_B = 122.33 \pm 0.22 \text{ km s}^{-1}$, $V_{\gamma,A} = 23.15 \pm 0.16 \text{ km s}^{-1}$ and $V_{\gamma,B} = 23.09 \pm 0.14 \text{ km s}^{-1}$, where the uncertainties in the systemic velocities do not include any transformation onto a standard system. The best fits are shown in Fig. 4. We cannot compare the K_A and K_B values directly with the results from T08 because they did not calculate these parameters explicitly.

We found an offset of $658 \pm 29 \text{ s}$ between the T_0 from the RV fit and that predicted from the ephemeris in Table II. Further investigation suggests that this offset is also present in the times of minimum light given by T08 and Hubscher et al.⁵⁷. As the current work is the first by the author that used the LIGHTKURVE package to access TESS data, one possibility is that this approach has caused an offset in the timestamps. We checked this by using LIGHTKURVE to download TESS light curves for ZZ UMa and ZZ Boo and compared them to those used in refs.⁵⁸ and⁵⁹. No offset in the timings was found, suggesting that the timing offset is an astrophysical effect, perhaps caused by a third component on a wider orbit around V570 Per.

V570 Per is present in the *Gaia* DR3 *Non-single-star orbital models for sources compatible with Double Lined Spectroscopic binary model* catalogue[§] which reports objects detected as double-lined and with a fitted spectroscopic orbit^{60,61}. The orbital parameters given are $e = 0.0029 \pm 0.0019$, $K_1 = 123.86 \pm 0.28 \text{ km s}^{-1}$ and $K_2 = 113.82 \pm 0.24 \text{ km s}^{-1}$, based on RVs from 24 spectra. The eccentricity is very small and consistent with zero, as expected. We find that K_2 is in good agreement with our K_A , but that K_1 is moderately discrepant with our K_B . It is clear that the identities of the stars have been swapped, but the source of the K_1/K_B discrepancy is unknown. We chose not to use these results because the spectra and RVs on which they are based are not publicly available so cannot be checked. It is relevant that Tokovinin⁶² has found issues with the *Gaia* DR3 K_1 and K_2 values in the sense that a significant fraction (14 of 22 in that case) have underestimated values or other problems.

[§]<https://vizier.cds.unistra.fr/viz-bin/VizieR-3?-source=I/357/tbosb2>

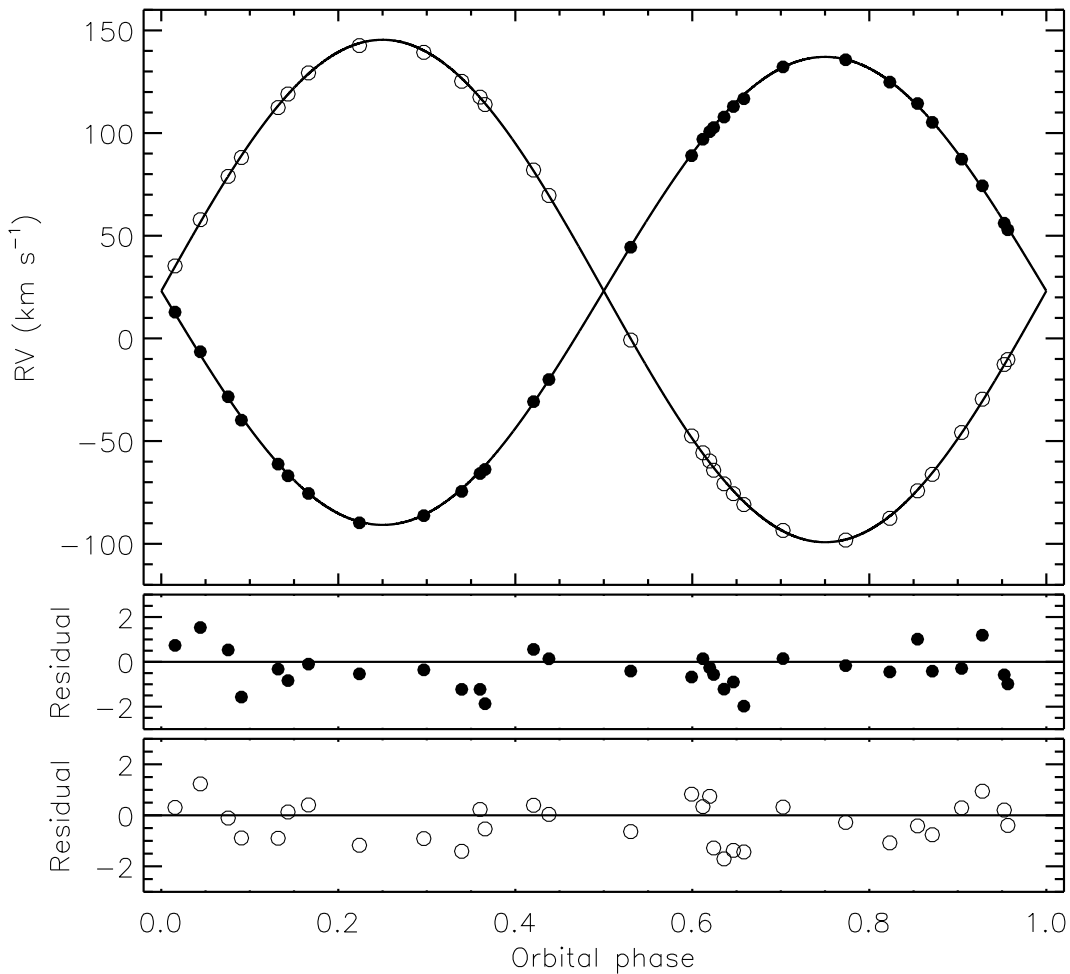


FIG. 4: RVs of V570 Per from T08 (filled circles for star A and open circles for star B) compared to the best-fitting spectroscopic orbits from our own analysis using JKTEBOP (solid curves). The residuals are given in the lower panels separately for the two components.

Physical properties of V570 Per

We determined the physical properties of V570 Per using the JKTEBOP code⁶³. The input values to this were: (i) the r_A , r_B , i and P from Table II; the K_A and K_B from the RV analysis; the T_{eff} values from T08 with the errorbars increased to ± 50 K to account for the systematic uncertainties of the T_{eff} scale for F-stars^{64–66}; an interstellar reddening of $E(B - V) = 0.05 \pm 0.02$ mag from the STILISM[¶] online tool^{67,68}; the B and V magnitudes from Tycho-2³¹ which are averages of 12 measurements at effectively random orbital phases; and the JHK_s magnitudes from 2MASS³² converted to the Johnson system using the transformations from Carpenter⁶⁹. The 2MASS magnitudes were taken at phase 0.10 so are representative of the average brightness of the system. The results are given in Table II, where the errorbars have been propagated individually from each input parameter.

[¶]<https://stilism.obspm.fr>

Table III: *Physical properties of V570 Per defined using the nominal solar units given by IAU 2015 Resolution B3 (ref. ⁷⁰).*

| <i>Parameter</i> | <i>Star A</i> | <i>Star B</i> |
|--|---------------------|---------------------|
| Mass ratio M_B/M_A | 0.9314 ± 0.0026 | |
| Semimajor axis of relative orbit (\mathcal{R}_\odot^N) | 9.100 ± 0.013 | |
| Mass (\mathcal{M}_\odot^N) | 1.4489 ± 0.0063 | 1.3495 ± 0.0062 |
| Radius (\mathcal{R}_\odot^N) | 1.538 ± 0.035 | 1.349 ± 0.032 |
| Surface gravity (log[cgs]) | 4.225 ± 0.020 | 4.308 ± 0.021 |
| Density (ρ_\odot) | 0.398 ± 0.027 | 0.550 ± 0.039 |
| Synchronous rotational velocity (km s ⁻¹) | 40.93 ± 0.92 | 35.89 ± 0.85 |
| Effective temperature (K) | 6842 ± 50 | 6562 ± 50 |
| Luminosity log(L/\mathcal{L}_\odot^N) | 0.669 ± 0.023 | 0.483 ± 0.024 |
| M_{bol} (mag) | 3.068 ± 0.058 | 3.533 ± 0.061 |
| Distance (pc) | 117.2 ± 2.3 | |

The agreement between the measurements in Table II and the results from T08 is good, with all quantities within 1σ . The radii of the stars have been determined to 2.3% precision, which is slightly worse than managed by T08 despite the availability of much better photometry for the current study. This arises because the precision of the radius measurements is limited by the spectroscopic light ratio applied in the photometric analysis, and perhaps from underestimated errorbars in T08. A better spectroscopic light ratio is needed to measure the radii more precisely.

The synchronous rotational velocities are consistent with the $v \sin i$ values measured by T08. This is in agreement with our assertion that the trends in the residuals of the fit to the light curves are due to starspots rotating synchronously with the orbit.

Inversion of the *Gaia* DR3 parallax gives a distance to the system of $d = 120.55 \pm 0.52$ pc, which is 1.4σ longer than that found in our own work via the *K*-band surface brightness method⁶³ and calibrations from Kervella et al.⁷¹. An increase in $E(B - V)$ to 0.1 mag would bring our optical (*BV*) and infrared (*JHK_s*) distances into better agreement at the expense of shortening the distance measurement to 115.8 ± 2.3 pc; this reddening is significantly more than the 0.023 ± 0.007 mag found by T08 from the interstellar sodium and potassium lines. The shorter distance could then be compensated by adopting larger T_{eff} values for the stars. The *Gaia* distance is questionable because the renormalised unit weight error (RUWE) of 1.395 for V570 Per is near the maximum value of 1.4 for a reliable astrometric solution²⁷.

Summary and conclusions

V570 Per is a dEB containing two F-type stars on a 1.90 d circular orbit. The system shows shallow (0.12 and 0.11 mag) partial eclipses which were discovered using the *Hipparcos* satellite. We used TESS light curves from two sectors and published RVs from T08 to determine its physical properties. The partial eclipses make a solution of the light curve alone poorly determined, but the addition of

a spectroscopic light ratio was sufficient to reach a determinate solution. The resulting radius measurements are relatively imprecise (2.3%) due to this, and in comparison with the mass measurements (0.5%). Our measured distance to the system is in reasonable agreement with that from *Gaia* DR3.

We compared the masses, radii and T_{eff} s of the stars to predictions from the PARSEC stellar evolutionary models⁷². The models provide a match to these properties to within the 1σ errorbars for an age of 800–900 Myr and a slightly supersolar fractional metal abundance of $Z = 0.020$ (where the solar value is $Z = 0.017$).

We also found the eclipses to arrive 11 min later than expected in the TESS light curves. Checks turned up no evidence for this being due to instrumental or data reduction issues, so it may be an astrophysical effect. The system should be monitored for eclipse timing variations caused by a possible third body. We also found residual systematics in the light curve which we attribute to weak starspots rotating synchronously with the orbit. Twenty-four observations with the *Gaia* Radial Velocity Spectrograph⁷³ yielded a double-lined spectroscopic orbit for the system which is in partial agreement with the ground-based results from T08. Future observations with *Gaia* should allow the addition of more RV measurements to this analysis, plus direct access to the *Gaia* spectra for checking the discrepancy found for one of the two stars.

Acknowledgements

We thank the anonymous referee for a quick and positive report. This paper includes data collected by the TESS mission and obtained from the MAST data archive at the Space Telescope Science Institute (STScI). Funding for the TESS mission is provided by the NASA’s Science Mission Directorate. STScI is operated by the Association of Universities for Research in Astronomy, Inc., under NASA contract NAS 5–26555. This work has made use of data from the European Space Agency (ESA) mission *Gaia*^{||}, processed by the *Gaia* Data Processing and Analysis Consortium (DPAC^{**}). Funding for the DPAC has been provided by national institutions, in particular the institutions participating in the *Gaia* Multilateral Agreement. The following resources were used in the course of this work: the NASA Astrophysics Data System; the SIMBAD database operated at CDS, Strasbourg, France; and the arXiv scientific paper preprint service operated by Cornell University.

References

- (1) D. M. Popper, *ARA&A*, **18**, 115, 1980.
- (2) J. Andersen, *A&ARv*, **3**, 91, 1991.
- (3) G. Torres, J. Andersen & A. Giménez, *A&ARv*, **18**, 67, 2010.
- (4) O. Y. Malkov *et al.*, *A&A*, **446**, 785, 2006.
- (5) Z. Eker *et al.*, *PASA*, **31**, e024, 2014.

^{||}<https://www.cosmos.esa.int/gaia>

^{**}<https://www.cosmos.esa.int/web/gaia/dpac/consortium>

- (6) J. Southworth, in *Living Together: Planets, Host Stars and Binaries* (S. M. Rucinski, G. Torres & M. Zejda, eds.), 2015, *Astronomical Society of the Pacific Conference Series*, vol. 496, p. 321.
- (7) J. Southworth, *Universe*, **7**, 369, 2021.
- (8) J. Andersen, J. V. Clausen & B. Nordström, *ApJ*, **363**, L33, 1990.
- (9) A. Claret & G. Torres, *A&A*, **592**, A15, 2016.
- (10) A. Claret & G. Torres, *ApJ*, **859**, 100, 2018.
- (11) T. Constantino & I. Baraffe, *A&A*, **618**, A177, 2018.
- (12) A. Tkachenko *et al.*, *A&A*, **637**, A60, 2020.
- (13) D. Graczyk *et al.*, *A&A*, **594**, A92, 2016.
- (14) G. Torres, *Astronomische Nachrichten*, **334**, 4, 2013.
- (15) Z. Jennings *et al.*, *MNRAS*, **521**, 3405, 2023.
- (16) G. Pietrzyński *et al.*, *Nature*, **567**, 200, 2019.
- (17) W. L. Freedman *et al.*, *ApJ*, **891**, 57, 2020.
- (18) J. Southworth, *The Observatory*, **140**, 247, 2020.
- (19) G. R. Ricker *et al.*, *Journal of Astronomical Telescopes, Instruments, and Systems*, **1**, 014003, 2015.
- (20) L. W. IJspeert *et al.*, *A&A*, **652**, A120, 2021.
- (21) A. B. Justesen & S. Albrecht, *ApJ*, **912**, 123, 2021.
- (22) A. Prša *et al.*, *ApJS*, **258**, 16, 2022.
- (23) F. van Leeuwen *et al.*, *A&A*, **323**, L61, 1997.
- (24) E. V. Kazarovets *et al.*, *IBVS*, **4659**, 1, 1999.
- (25) U. Munari *et al.*, *A&A*, **378**, 477, 2001.
- (26) L. Tomasella *et al.*, *A&A*, **483**, 263, 2008.
- (27) Gaia Collaboration, *A&A*, **649**, A1, 2021.
- (28) A. J. Cannon & E. C. Pickering, *Annals of Harvard College Observatory*, **91**, 1, 1918.
- (29) ESA (ed.), *The Hipparcos and Tycho catalogues. Astrometric and photometric star catalogues derived from the ESA Hipparcos space astrometry mission, ESA Special Publication*, vol. 1200, 1997.
- (30) K. G. Stassun *et al.*, *AJ*, **158**, 138, 2019.
- (31) E. Høg *et al.*, *A&A*, **355**, L27, 2000.
- (32) R. M. Cutri *et al.*, *2MASS All Sky Catalogue of Point Sources* (The IRSA 2MASS All-Sky Point Source Catalogue, NASA/IPAC Infrared Science Archive, Caltech, US), 2003.
- (33) Lightkurve Collaboration, ‘(Lightkurve: Kepler and TESS time series analysis in Python)’, *Astrophysics Source Code Library*, 2018.
- (34) J. M. Jenkins *et al.*, in *Proc. SPIE*, 2016, *Society of Photo-Optical Instrumentation Engineers (SPIE) Conference Series*, vol. 9913, p. 99133E.
- (35) J. Southworth, P. F. L. Maxted & B. Smalley, *MNRAS*, **351**, 1277, 2004.
- (36) J. Southworth, *A&A*, **557**, A119, 2013.
- (37) G. Torres *et al.*, *AJ*, **120**, 3226, 2000.
- (38) J. Southworth, H. Bruntt & D. L. Buzasi, *A&A*, **467**, 1215, 2007.
- (39) J. Southworth, *The Observatory*, **141**, 52, 2021.
- (40) J. Southworth, S. J. Murphy & K. Pavlovski, *MNRAS*, **520**, L53, 2023.
- (41) F. Allard, D. Homeier & B. Freytag, *Philosophical Transactions of the Royal Society of London Series A*, **370**, 2765, 2012.
- (42) J. Southworth, *The Observatory*, **143**, 71, 2023.
- (43) D. Hestroffer, *A&A*, **327**, 199, 1997.
- (44) A. Claret & J. Southworth, *A&A*, **664**, A128, 2022.
- (45) P. F. L. Maxted, *A&A*, **616**, A39, 2018.
- (46) J. Southworth, P. F. L. Maxted & B. Smalley, *MNRAS*, **349**, 547, 2004.
- (47) J. Southworth, *MNRAS*, **386**, 1644, 2008.
- (48) J. Wang *et al.*, *MNRAS*, **504**, 4302, 2021.

- (49) J. Southworth, *The Observatory*, **142**, 103, 2022.
- (50) P. Lenz & M. Breger, in *The A-Star Puzzle*, Cambridge University Press, Cambridge, UK. (J. Zverko, J. Žižnovský, S. J. Adelman, & W. W. Weiss, ed.), 2004, *IAU Symposium*, vol. 224, pp. 786–790.
- (51) P. Gaulme & J. A. Guzik, *A&A*, **630**, A106, 2019.
- (52) J. Southworth, *The Observatory*, **141**, 282, 2021.
- (53) J. Southworth & T. Van Reeth, *MNRAS*, **515**, 2755, 2022.
- (54) F. Kahraman Açıcaş et al., *RAA*, **22**, 085003, 2022.
- (55) X. Chen et al., *ApJS*, **263**, 34, 2022.
- (56) J. Southworth, *The Observatory*, **141**, 234, 2021.
- (57) J. Hubscher et al., *IBVS*, **5918**, 1, 2010.
- (58) J. Southworth, *The Observatory*, **143**, 19, 2023.
- (59) J. Southworth, *The Observatory*, **142**, 267, 2022.
- (60) Gaia Collaboration, *A&A*, **595**, A1, 2016.
- (61) Gaia Collaboration, *arXiv:2206.05595*, 2022.
- (62) A. Tokovinin, *AJ*, in press, *arXiv:2304.02706*, 2023.
- (63) J. Southworth, P. F. L. Maxted & B. Smalley, *A&A*, **429**, 645, 2005.
- (64) M. De Pascale et al., *A&A*, **570**, A68, 2014.
- (65) T. Ryabchikova et al., *MNRAS*, **456**, 1221, 2016.
- (66) P. Jofré, U. Heiter & C. Soubiran, *ARA&A*, **57**, 571, 2019.
- (67) R. Lallement et al., *A&A*, **561**, A91, 2014.
- (68) R. Lallement et al., *A&A*, **616**, A132, 2018.
- (69) J. M. Carpenter, *AJ*, **121**, 2851, 2001.
- (70) A. Prša et al., *AJ*, **152**, 41, 2016.
- (71) P. Kervella et al., *A&A*, **426**, 297, 2004.
- (72) A. Bressan et al., *MNRAS*, **427**, 127, 2012.
- (73) M. Cropper et al., *A&A*, **616**, A5, 2018.